An Innovative Adaptive Droop Control Based on Available Energy for DC Micro Distribution Grids [†]

Duc Nguyen Huu

Department of Renewable Energy, Faculty of Energy Technology, Electric Power University, 235—Hoang Quoc Viet, Hanoi 11355, Vietnam; ducnh@epu.edu.vn; Tel.: +84-901008555

[†] This paper is an extended version of our paper published in: Duc, N.H.; Hung, T.N. Adaptive Coordinated Droop Control for Multi-Battery Storage. In Proceedings of the IEEE EUROCON 2015—International Conference on Computer as a Tool (EUROCON), Salamanca, Spain, 8–11 September 2015.

check for updates

Abstract: DC distribution grids are increasingly a promising solution for wind and solar integration due to good matching with DC output voltage such as photovoltaic (PV) array systems, distributed battery storage systems (BESS) and electric vehicles. To overcome the control problems involving coordination control schemes of multi-BESSs in real-time as well as operation strategies of DC grids in the long-term, this paper presents the effective adaptive coordinated droop control of multi-battery energy storage systems (MBESSs) in DC distribution grids. The adaptive coordinated droop is proposed according to the available energy levels in BESSs. With the proposed method, the ual-objectives, which are stabilization of DC voltages especially through disturbance for instance outage of BESS and enhancement of State of Charge (SOC)-balance speed among BESSs, can be achieved. Analytical derivations are established to investigate the impacts of the adaptive method. Meanwhile, the influence of the proposed method on the stability is presented.

Keywords: adaptive droop control; state of charge; small-signal stability; eigenvalue; wind turbine; photovoltaic; battery storage; super-capacitor; cache control

1. Introduction

In recent years, small-scaled networks based on renewable energy resources (RES) including photovoltaic array, wind power generation combined energy storage systems are of an increasingly great interest [1–3]. Concept of a net zero-energy building is introduced to harvest energy from wind and solar in urban areas [4–6]. With such buildings, electricity consumption from the main grid can be reduced through the balance between generated clean energy and demand. Integration of solar and wind into buildings is studied in [7,8]. For such green buildings, the DC grid is a good choice because of its inherent advantage for DC output voltage such as photovoltaic (PV) arrays, DC loads and battery energy storage systems (BESS). Due to many advantages, DC grid integrated distributed sources are considered as an attractive choice [9]. On comparison with AC microgrid, DC microgrid can eliminate DC–AC or AC–DC power conversion stages of renewable sources and loads, therefore not only the size and cost of the DC system could be reduced but also its efficiency could be increased [10]. For those aforementioned reasons, several studies have investigated the deployment of DC distribution network [11,12].

In order to ensure operation of DC grids, power balance between power supply side and load demand must be matched. For such DC grids, the power balance regulation can be implemented by the DC voltage control and power quality management [13,14]. Recently, the control methods for power electronic converters in dc distribution grids have been intensively reported. Among them, the DC voltage droop control is widely considered as the attractive method to integrate several distributed

generation sources in DC grids [15–20]. The merit of this method is to balance the power supply and demand side without high-speed communication network. Fundamentally, by applying the droop control, it reduces the output voltage reference when the output power increases. The output power of the distributed generation unit should be inversely proportional to its droop coefficient. For the conventional droop control, fixed values of the droop constants are typically based on the power ratings. However, it does not consider the actual energy levels in BESSs. Moreover, it is not proper to use the same virtual resistance for BESSs with different capacities or actual SOCs. In [21], a SOC-based droop method is used to share dynamic power among distributed energy storage units in AC microgrid applications. In [22,23], the frequency of islanded AC microgrids is employed to adjust the charging/discharging rate of each battery. In [24,25], the gain-scheduling droop is determined according to the SOC of batteries. The ideas in such publications are that the battery with higher SOC should provide more power and the battery with less SOC should provide less. Since a good life-cycle for batteries is expected as small depth of discharge (DOD) as possible [26], thus, the SOCs of all batteries under its droop control in the system should be equalized for their good lifetime. It is therefore desirable that the BESS should participate in DC voltage stabilization depending on the available energy level (difference between the current energy level and the scheduled minimum level). At the same, the SOCs of BESSs could be equal in the long-term operation.

To achieve these objectives, the advanced coordinate droop control scheme is presented. It is proposed that an adaptive virtual resistance (*AVR*) is determined based on a function of the normalized available energy amount (SOC_{ava}) depending on the real-time SOC and minimum permitted energy level of $BESS_i$. The idea is that the participation factor of each BESS into DC voltage stabilization should take consideration not only the power ratings but also the available energy levels that BESS can support. With this proposed method, BESSs, which are already operating very close to the operating limit, should not participate much in DC voltage stabilization. Moreover, BESS with higher SOC_{ava} should have a higher discharge rate and vice versa. Therefore, in the discharging process, a higher *AVR* should be given to a battery with lower SOC_{ava}. On the other hand, during the charging process, higher *AVR* should be given to a battery with higher SOC_{ava}. As a result, a symmetric function determining *AVR* for the charge and discharge process can be devised. Thus, it enhances the SOC-balancing speed among BESSs without the communication requirement among themselves.

Furthermore, one of the emerging issues is how the adaptive droop scheme impacts the overall stability of DC distribution systems. The impacts of the droop control loop on the stability for multi-terminal DC (MTDC) grids are reported in [27]. However, in [27], the models of distributed generation units such as wind, PV, BESS generations are not taken into account. Thus the influence of SOCs and the interaction between electric units could not be investigated. For the proposed adaptive droop control, it is essential to define the stable region through eigenvalues analysis taking into count all distributed renewable units, which will be performed in this paper.

One of the key contributions in the paper is that the analytical method is presented to study the impacts of the proposed adaptive control on DC grids during transient as well as long-term operation. Moreover, the effect of the proposed droop method on the stabilization of the DC bus voltage in real-time during disturbance especially outage of converter is also investigated.

The rest of the study is organized as follows: Section 2 describes the DC distribution grid configuration and its control strategy. Model of the BESS is briefly presented and the voltage droop control also is revised. The adaptive coordinated droop control and its analysis are discussed in Section 3. Analysis of limitations and impacts is carried out in Section 4. Section 5 provides a small signal analysis, which is a necessary supplement to determine the proper range of the exponent coefficients in the AVR function in order to ensure the system stable. Simulation results are given in Section 6 to verify the method. The conclusions are summarized in Section 7.

2. DC Distribution Microgrid

Schematic of the DC distribution system introduced in [28] is adapted in this work as shown in Figure 1. It is composed of a wind energy conversion system (WECS), PV arrays, distributed battery storage systems (BESSs), super-capacitor storage, variety of loads and electronic power converters that connect distributed generation units into DC grid. The WECS includes a wind turbine and a permanent magnet synchronous generator connected to the DC grid through a buck converter. The PV unit consists of a PV array and a buck converter. The super-capacitor is used to compensate fast fluctuations by using the cache control concept [29–38]. BESSs and the super-capacitor are integrated with the DC grid through a bidirectional buck converter. The overall presented control scheme of the DC grid is hierarchical and divided into three layers: the primary control; the converter control system and the distribution management system level (DSM). The primary control aims for controlling in each distributed generation units such as the battery management system. The DSM level is to coordinate the different operation modes and perform the optimized operation strategies. The converter control system is composed of two control loops: the outer loop providing a current reference for the inner one and the later regulates the output current to keep track of the reference. The scope of this paper is to develop the adaptive coordinated droop control at the converter level.
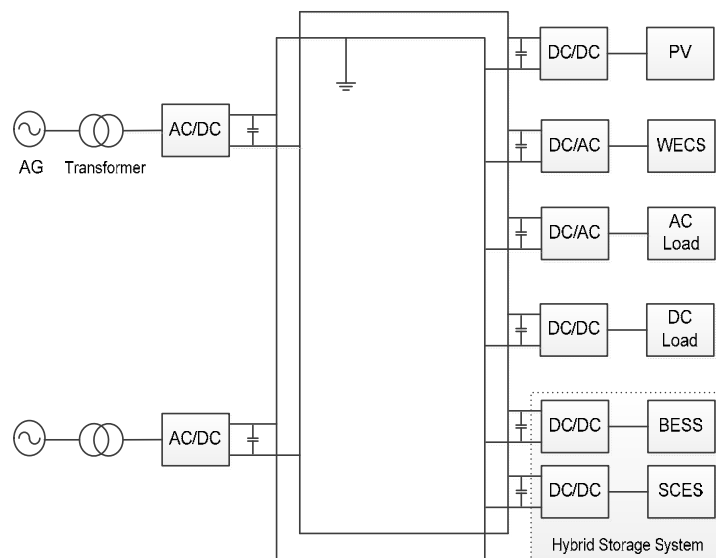

Figure 1. Typical loop configuration of the DC micro-distribution grid.

2.1. Conventional Droop Control Method

The DC voltage droop control is based on the droop characteristic of converter. Basically, the DC voltage reference is changed by adjusting the virtual resistance, thus regulating the power-sharing among distributed generation units. The concept is similar with the power-frequency droop characteristic applied for synchronous generations in AC grids. The method takes full merit of distribution characteristic of such DC distribution grids and has the high reliability [27–29]. Figure 2 shows the adaptive droop concept based on available state of charge of batteries. The feedback loop is applied to provide the DC voltage reference for the inner control loop. The DC voltage reference can be adjusted by changing the virtual resistance.

$$V_{dcdroop} = V_{dcref} - R_{VR} \times I_{BESS} \qquad (1)$$

There are two special virtual resistances: the zero value corresponding to the voltage source converter (VSC) mode and the infinite value that corresponds to the current source converter (CSC) mode. Hence, a constant power load and constant power source are instances of the CSC mode. PV and WECS are normally operated in the maximum power point tracking (MPPT) scheme to exploit

maximum possible power from clean generation sources. Thus, in normal condition operation, WECS and PV are considered as the CSC mode. Distributed BESSs are operated according to the droop control to regulate DC voltage. The DC grid is connected to the AC grid through DC/AC converter in interconnected mode. The virtual resistance of the grid converter is set to stabilize DC voltage when the BESSs are not sufficient.
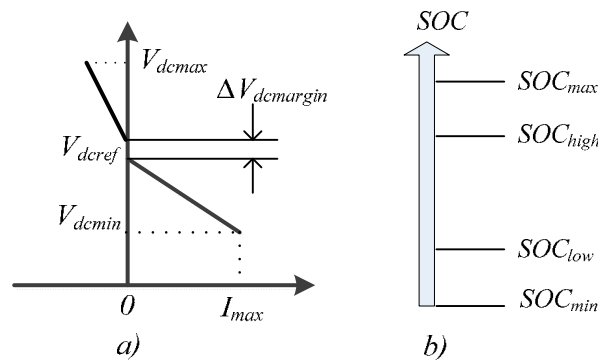

Figure 2. (**a**) Droop control method and (**b**) boundary level SOC of a battery storage system (BESS).

2.2. Model of the Battery Energy Storage System (BESS)

As aforementioned in the previous section, the purpose of the research is to propose an adaptive coordinated droop control for BESSs in dc distribution grids. Hence, a model of BESS is briefly presented as shown in Figure 3.
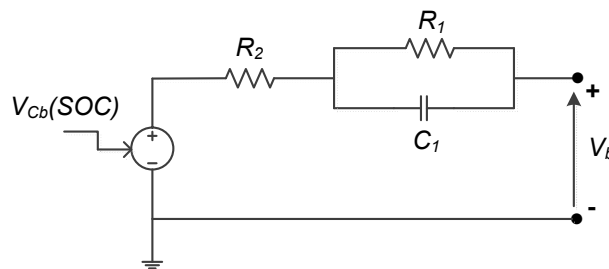

Figure 3. Simplified circuit battery model.

The battery energy storage system (BESS) is a significant component of the DC distribution network to effectively utilize or store energy in the system. BESS is composed of the battery and a DC/DC converter. In the research, the model in [31] is employed because this model represents most of the important characteristics of the battery. The validated electrical circuit model reported in [31] meets all requirements for a good battery model. In this model most nonlinear battery element characteristics in the charging and discharging process as well as their dependence on the state of charge (SOC) of the battery are taken into account. As a result, the model of the BESS can be expressed as follows:

$$V_{C_b}(SOC) = V_{C_b}^0 - K_e(1 - SOC) \tag{2}$$

$$\dot{V}_{C_1} = -\frac{1}{C_1 R_2}V_{C_b} - \frac{1}{C_1}\left(\frac{1}{R_1} + \frac{1}{R_2}\right)V_{C_1} + \frac{1}{C_1 R_2}V_b \tag{3}$$

where $V_{C_b}^0$ is the open-circuit voltage when the battery is fully charged. Meanwhile, the *SOC* of the battery can be calculated as:

$$SOC_i(t) = SOC_i(0) - \int_0^t \eta \frac{i_{BT,i}(\tau)}{E_{BT,i}}d\tau \tag{4}$$

where $i_{BT,i}$ is the battery current, $SOC_i(0)$ is the initial value SOC of $BESS_i$, $E_{BT,i}$ is the capacity of battery and η is the charging or discharging efficiency.

3. Innovative Adaptive Droop Method

3.1. Concept of Adaptive Coordinate Droop Control

For the conventional droop control, fixed or preset values of the virtual resistances are typically calculated according to the power ratings of BESSs, it does not consider the actual energy levels and hence the available energy amount of BESSs for stabilizing the DC voltage during the steady state and transients caused by different kinds of contingency. In order to solve the problem, an effective adaptive coordinate droop control is proposed. In this novel method, the adaptive droop virtual resistance (AVR) is automatically determined based on the actual available energy amount of BESSs.

A symmetric function determining AVR_i taking into an account $SOCs$ of batteries is expressed as.

$$AVR_{charge,i} = R_{VR0}\frac{E_{BT,i}}{E_{max}}SOC_{ava,i}^q \tag{5}$$

$$AVR_{discharge,i} = R_{VR0}\frac{E_{BT,i}}{E_{max}}SOC_{ava,i}^{-q} \tag{6}$$

where $SOC_{ava,i}$ is the normalized available energy amount of the ith BESS, which can be determined as:

$$SOC_{ava,i} = \frac{SOC_i - SOC_{min,i}}{SOC_{low,i} - SOC_{min,i}} \tag{7}$$

where SOC_i, $SOC_{low,I}$ and $SOC_{min,i}$ are the real-time state of charge at time t, the low state of charge and minimum state of charge of the ith BEES, respectively; R_{VR0} is the nominal virtual resistance in the fixed droop control and $E_{BT,I}$ and E_{max} are the nominal capacity of the ith BESS and the maximum capacity of BESSs in the system, respectively.

The reason for using the exponential rather than linear function is to get the faster balancing for SOCs. The exponent q in Equation (5) is determined to stabilize the DC voltage as well as adjust the SOC-balancing speed among BESSs, which are discussed in more detail in the following subsections. Furthermore, the BESSs with close to the permitted minimum SOC should not contribute much on DC voltage stabilization.

It is also envisioned that if the DC distribution networks joint to the electricity market in the future, the BESS owners may want to use an energy reserve of BESS as an ancillary service [32]. Thus the SOC_{min} can be set based on the optimal operation strategies. Therefore, due to both technical and market aspect related limitations, the adaptive coordinate droop control scheme is of an importance solution for DC distribution networks in the future.

The hierarchical control scheme of the ith BESS is depicted in Figure 4, in which there are three control layers. The SOC balancing of each cell in BESS and temperature and battery voltage monitoring are performed in the battery management system layer. The long-term operation mode and strategies of the DC grid and change of operation modes are carried out in the distribution management system (DSM). Depending on the operation mode and strategies, the minimum energy level of BESS can be a SOC_{min} in respect to the technical limit or a value determined according to the long-term operation strategy for instance an energy reserve amount for ancillary services. In order to regulate the charge and discharge processes of the BESS unit, the converter control system layer including the adaptive droop control as shown in Figure 5 was used. In addition, the variable droop loop that generates the voltage reference for the voltage control loop, the control scheme employs two further control loops, which are an inner current control loop and an outer voltage control loop, both of which are a proportional-integral (PI) controller. The equations for this control system are given as follows:

$$I_{b\_refP} = K_{PaBT}(V_{dc} - V_{dcref}) \tag{8}$$

$$\dot{I}_{b\_refI} = K_{IaBT}(V_{dc} - V_{dcref}) \tag{9}$$

$$I_{b\_ref} = I_{b\_refP} + \dot{I}_{b\_refI} \tag{10}$$

$$d_{PBT} = K_{PbBT}(I_{b\_ref} - I_b) \tag{11}$$

$$\dot{d}_{IBT} = K_{IbBT}(I_{b\_ref} - I_b) \tag{12}$$

$$d_{BT} = d_{PBT} + d_{IBT} \tag{13}$$

where I_{b_ref} is the reference current achieved from the voltage control loop and d_{BT} is the average duty ratio of the converter; the subscript "P" and "I" represent the proportional component and the integral component of the duty ratio, respectively.
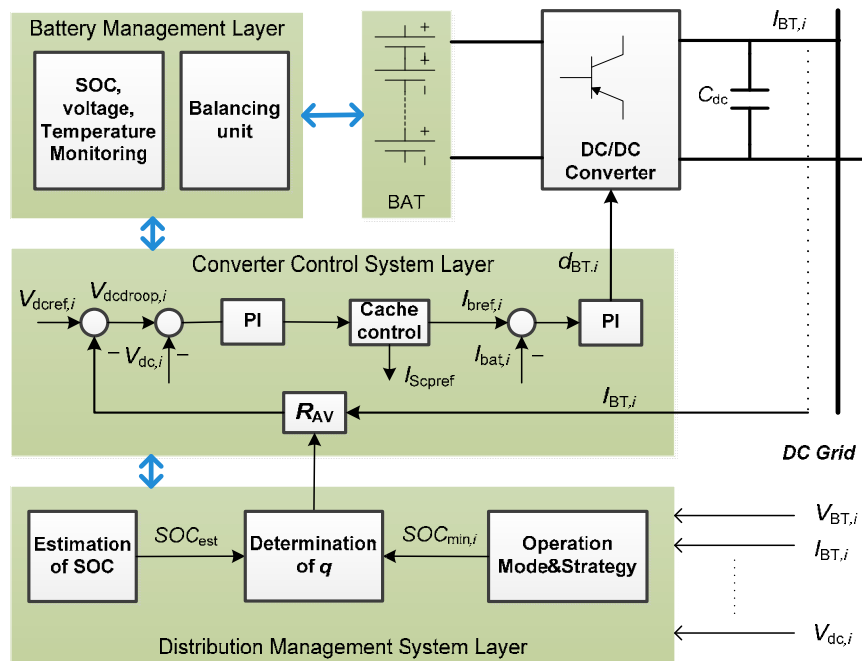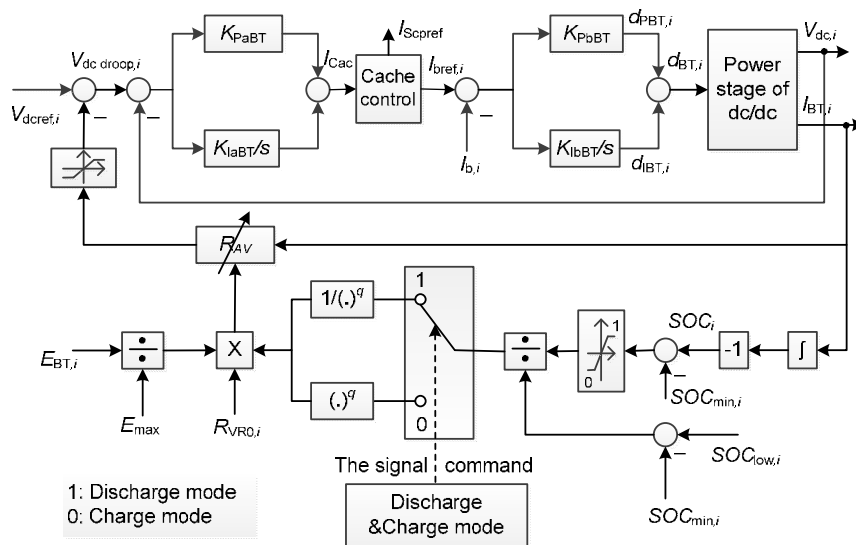

Figure 4. Control diagram of the *i*th BESS.

Figure 5. Diagram of the proposed control system for the *i*th BESS.

3.2. Effect of the Proposed Method on Stabilizing the DC Voltage

In this subsection an analytical derivation of the effect of the adaptive coordinate droop control on stabilizing the DC voltage is presented. This analysis is also applicable for contingency such as outage of converter connected to BESS.

The equation expressing the droop control law for the *i*th BESS can be written as:

$$I_{BESS,i} = I^0_{BESS,i} - \frac{1}{AVR_i}(V_{dc,i} - V^0_{dc}) \tag{14}$$

$$\Delta I_{BESS,i} = -\frac{1}{AVR_i}\Delta V_{dc,i} \tag{15}$$

where

$$\Delta I_{BESS,i} = I_{BESS,i} - I^0_{BESS,i} \tag{16}$$

$$\Delta V_{dc,i} = V_{dc,i} - V^0_{dc,i} \tag{17}$$

For stabilization of the DC voltage, BESSs must compensate the fluctuation of the powers in the system, which is caused by with the assumption increase of current ΔI_{Fluc}. Using Equations (14) and (15), the current compensation of BESSs can be described as:

$$\sum_{i=1}^{n} \Delta I_{BESS,i} = \Delta I_{Fluc} \tag{18}$$

$$\sum_{i=1}^{n} g_{AVR,i}\Delta V_{dc,i} = -\Delta I_{Fluc} \tag{19}$$

$$\Delta I_{BESS,i} = g'_{AVR,i}\Delta I_{Fluc} \tag{20}$$

where

$$g'_{AVR,i} = \frac{g_{AVR,i}\Delta V_{dc,i}}{\sum\limits_{k=1}^{n} g_{AVR,k}\Delta V_{dc,k}} \tag{21}$$

Replacing AVR from the Equation (6), the Equation (21) can be rewritten as

$$g'_{AVR,i} = \frac{g^0_i SOC^q_{ava,i}\Delta V_{dc,i}}{E_{BT,i}\sum\limits_{k=1}^{n} g^0_k SOC^q_{ava,k}\Delta V_{dc,k}/E_{BT,k}} \tag{22}$$

where $g'_{AVR,i}$ is the modified virtual conductance for the *i*th BESS, g^0_i and $g_{AVR,i}$ are the defined as the inverse of the virtual resistance in the fixed droop control and the adaptive droop control respectively.

Substitute Equation (22) into Equation (20) the actual compensation of the *i*th BESS can be determined as

$$\Delta I_{BESS,i} = \frac{g^0_i SOC^q_{ava,i}\Delta V_{dc,i}}{E_{BT,i}\sum\limits_{k=1}^{n} g^0_k SOC^q_{ava,k}\Delta V_{dc,k}/E_{BT,k}}\Delta I_{Fluc} \tag{23}$$

If it is assumed that there is lossless or the common voltage feedback signal used instead of local voltages, as in (22) the relative virtual conductance of the *i*th BESS for stabilizing DC voltage can be written as

$$g'_{AVR,i} = \frac{g^0_i SOC^q_{ava,i}}{E_{BT,i}\sum\limits_{k=1}^{n} g^0_k SOC^q_{ava,k}/E_{BT,k}} \tag{24}$$

Neglecting the losses, it is drawn from Equation (23) and Equation (24) that for a fixed droop control and BESSs with equal ratings (it leads to equal virtual resistance or equal conductance) the compensates from all the BESSs are equally by $\Delta I_{BESS,i} = \Delta I_{Fluc}/n$. According to the above analysis derivations, it can be concluded that the actual compensation of the *i*th BESS depends on the available energy levels in BESSs. The participation of the $BESS_i$ on DC voltage stabilization is therefore dependent on the available energy levels, which impedes a straightforward analysis.

Let us consider an important contingency case for instance an outage of converter connected to $BESS_i$, it is assumed that in the steady state before the outage, the $BESS_i$ supplies the current of $I_{BESS,i}^0$, hence the participation of the other BESSs into power redistribution, which can be described as

$$\Delta I_{BESS,j} = g'_{AVR,j} I_{BESS,i}^0 \tag{25}$$

where

$$g'_{AVR,j} = \frac{g_j^0 SOC_{ava,j}^q \Delta V_{dc,j}}{E_{BT,j} \sum\limits_{\substack{k=1 \\ k \neq i}}^{n} g_j^0 SOC_{ava,j}^q \Delta V_{dc,j} / E_{BT,k}} \tag{26}$$

in case of the general case

$$\text{or } g'_{AVR,j} = \frac{g_j^0 SOC_{ava,j}^q}{E_{BT,j} \sum\limits_{\substack{k=1 \\ k \neq i}}^{n} g_j^0 SOC_{ava,j}^q / E_{BT,k}} \tag{27}$$

in case of lossless or the common voltage feedback signal used.

Now, let us consider how the adaptive coordinate droop scheme works for the whole DC distribution system. The DC system equations describing the relation between the current and the node voltage can be written in a matrix form as

$$Y_{dc} V_{dc} = I_{dc} \tag{28}$$

where $I_{dc} = [I_{WT}, I_{PV}, I_{Load}, I_{AG}, I_{BESS1}, I_{BESS2}, \ldots]^T$ containing the currents flowing into the DC network; V_{dc} is the DC bus voltage vector and Y_{dc} is the DC network admittance matrix. The current and voltage vector can be rewritten as

$$V_{dc} = V_{dc}^0 + \Delta V_{dc} \tag{29}$$

$$I_{dc} = I_{dc}^0 + \Delta I_{dc} \tag{30}$$

Then the DC network equations can be expressed as

$$Y_{dc} \Delta V_{dc} - \Delta I_{dc} = I_{dc}^0 - Y_{dc} V_{dc}^0 \tag{31}$$

where "0" indicates the steady state of the DC system before disturbances.

According to Equation (19), we have

$$\Delta I_{dc} = -G \Delta V_{dc} \tag{32}$$

where G is the diagonal matrix composed of the conductance g_i and can be expressed as

$$G = diag\left([g_{WT}, g_{PV}, g_{AG}, g_{Load}, g_{AVR1}, \cdots g_{AVRn}]\right) \tag{33}$$

Replacing the current and voltage V_{dc}^0 and I_{dc}^0 with the values corresponding to the situation before the disturbance, and substituting Equation (31), the DC network equation becomes:

$$(Y_{dc} + G) \Delta V_{dc} = 0 \tag{34}$$

So (34) is the DC system equation describing the DC system after disturbance. There is only trivial solution $\Delta V_{dc} = 0$ for Equation (34) provided that $\det(Y_{dc} + G) \neq 0$. When a distributed generation unit for example WT, PV block will be controlled under the constant current method, the conductance of these distributed units will equal zero. Therefore, the matrix G can be rewritten as:

$$G = \begin{bmatrix} 0 & 0 & 0 & 0 \\ 0 & g_{AVR,1} & 0 & 0 \\ 0 & 0 & \ldots & 0 \\ 0 & 0 & 0 & g_{AVR,n} \end{bmatrix} \tag{35}$$

So, the matrix G after disturbances can be expressed as

$$G' = diag\left(\left[g'_{AVR,1}, \ldots, g'_{AVR,i}, \ldots, g'_{AVR,n}\right]\right) \tag{36}$$

Similarly, in case of an outage of the $BESS_i$, the matrix G can be defined as

$$G' = diag\left(\left[g'_{AVR,1}, \ldots, g'_{AVR,i-1}, 0, g'_{AVR,i+1}, \ldots, g'_{AVR,n}\right]\right) \tag{37}$$

Applying the superposition principle, the voltage deviations after disturbances can be calculated by solving the equation as:

$$(Y_{dc} + G')\Delta V_{dc} = I_{dc,Fluc} \tag{38}$$

where the matrix Y'_{dc} is a modified admittance matrix and along with the current disturbance vector $I_{dc,Fluc}$ can be defined as

$$Y'_{dc} = Y_{dc} + G' \tag{39}$$

$$I_{dc,Fluc} = \left[0, \ldots, \Delta I_{Fluc,i}, \ldots, 0\right] \tag{40a}$$

in case of a power change at node i

$$I_{dc,Fluc} = \left[0, \ldots, -I^0_{BESS,i}, \ldots, 0\right] \tag{40b}$$

in case of an outage of the $BESS_i$

The matrix G' expresses the effect of the adaptive virtual resistance on the voltage deviations caused by disturbances. Hence, the change of the output currents in BESSs can thereafter be calculated from

$$\Delta I_{BESS} = Y_{dc}\Delta V_{dc} = -G'\Delta V_{dc} \tag{41}$$

where the redistributed output current vector of the BESSs is

$$\Delta I_{BESS} = [\Delta I_{BESS,1}, \ldots, \Delta I_{BESS,i}, \ldots, \Delta I_{BESS,n}] \tag{42}$$

It is seen from Equation (24) that with the lossless assumption, the matrix G is independent of the DC grid topology. However, with DC line voltage drop consideration the analytical derivations are obviously more accurate and provide the impact of the prosed method on the interaction among *BESSs*. It is noted that with decreasing the available energy levels will lead to a more uniform voltage deviation profile but larger voltage deviation. It can be seen that when the higher q is chosen, the faster equalization of SOC can be achieved. However, for the influence of q into the DC voltage deviation, it is more complicated: it is remarked from Equation (15) and Equation (25) that increasing the exponent coefficient q when the SOC is higher than SOC_{low} results in smaller DC voltage deviation but increasing the q when the SOC in range of SOC_{min} to SOC_{low}, the DC voltage deviation is larger. However, it could adversely cause the system to be unstable as discussed later in Section 5.

3.3. Effect of the Proposed Method on the State of Charge Balance

In this subsection, the influence of the proposed method on power sharing and state of charge balancing speed among BESSs in long-term operation is discussed.

It is obviously seen that the value of AVR should be inversely proportional to the output power of BESSs. Hence, when the $AVR_{discharge,i}$ is formulated to be inversely proportional to the available energy amount $SOC^q_{ava,i}$, the output power of each BESS will be proportional to the $SOC^q_{ava,i}$. In contrary consideration, $AVR_{charg,ie}$ is formulated to be proportional to the $SOC^q_{ava,i}$. In other words, with the AVR_i concept the BESS with a higher available energy amount will discharge more power and charge less power, while the ones with lower $SOC^q_{ava,i}$ will discharge less power and charge more power. As a consequence, after a dynamic process the SOC balancing among BESSs is achieved. Therefore, the proposed method makes the SOC-balancing speed faster. The SOC balancing speed can be adjusted by changing the exponent coefficient q in Equation (5) and Equation (6).

The output currents of the BESSs follow the relationship:

$$\sum I_{BESS,i} = I_{Load} + I_{loss} \tag{43}$$

$$I_{Load} = \sqrt{\frac{P_L}{R_L}} = \frac{V_{dc,L}}{R_L} \tag{44}$$

where I_{Load} is the required load current and is equal the aggregated exchange current of the all BESSs minus the total loss in the dc grid I_{loss}; P_L is the load power demand and $V_{dc,L}$ is the voltage of load. It is assumed to model the load as the resistance R_L.

By combining Equation (18), Equation (43) and Equation (44), we have:

$$\sum_{i=1}^{n} g_{AV,i} \Delta V_{dc,i} = \frac{V_{dc,L}}{R_L} \tag{45}$$

$$I_{BT,i} = \frac{g_i^0 SOC^q_{ava,i} \Delta V_{dc,i}}{E_{BT,i} \sum\limits_{k=1}^{n} (g_i^0 SOC^q_{ava,k} \Delta V_{dc,k} / E_{BT,k})} \times \frac{V_{dc,L}}{R_L} \tag{46}$$

Therefore, the aggregated required load can be dynamically shared according to available energy amount $SOC_{ava,i}$ of the BESSs. Considering Equation (46), Equation (4) can be rewritten as:

$$SOC_i(t) = SOC_i(0) - \int_0^t \eta \frac{g_i^0 SOC^q_{ava,i} \Delta V_{dc,i}}{E^2_{BT,i} \sum\limits_{k=1}^{n} (g_i^0 SOC^q_{ava,k} \Delta V_{dc,k} / E_{BT,k})} \frac{V_{dc,L}}{R_L} d\tau \tag{47}$$

4. Limitation and Impact of the Exponent Coefficient

As discussed in the previous sections, the SOC-equalization speed as well as the dynamic deviation of the DC voltage during transients can be regulated by adjusting the exponent coefficient q. In order to determine the accepted range of the exponent coefficient, the following constraints must be satisfied.

(1) The output currents of BESSs must be smaller than the maximum permitted output current of each BESS, it is hence expressed as:

$$I_{BESS,i}(t) \le I_{max,i} \tag{48}$$

Due to the limitation of the maximum permitted output current of each DESS, it is obtained as

$$\frac{g_i^0 SOC^q_{ava,i} \Delta V_{dc,i}}{E_{BT,i} \sum\limits_{k=1}^{n} g_i^0 SOC^q_{ava,k} \Delta V_{dc,k} / E_{BT,k}} \le \frac{R_L}{V_{dc,L}} I_{max,i} \tag{49}$$

Inequality (49) will determine the first limitation of the exponent coefficient. If q is larger than its upper limit, the output current of the BESS will exceed its maximum permitted current of the converter. It is noted that the upper limit value is dependent on the load condition as well as the available energy levels in all BESSs. In this paper, all analytical derivations are established with consideration that there will be n DBESSs in DC distribution grids. However, in order to get an illustrative example, it is assumed two BESSs with the same power ratings and capacities connected to the DC grid. Figure 6 shows the relationship between the output currents and their exponent q. The system parameters are listed in the Appendix A.
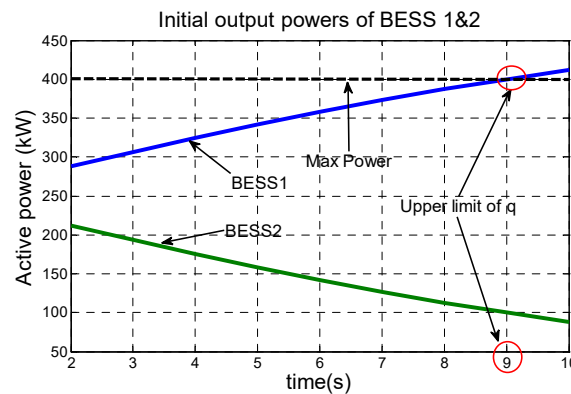

Figure 6. The relationship between the coefficient q and the output powers of BESSs.

(2) The second constraint that determines the exponent coefficient is the maximum permitted DC voltage deviation due to the droop control. Neglecting the lossless, the DC voltage deviation in charge and discharge respectively can be acquired from Equation (5), Equation (6) and Equation (45) as.

$$\Delta V_{dc} = \frac{1}{\sum\limits_{i=1}^{n} SOC_{ava,i}^{q} / m_i} \times \frac{V_{dc,L}}{R_L} \tag{50}$$

in case of the discharge progress

$$\Delta V_{dc} = \frac{1}{\sum\limits_{i=1}^{n} SOC_{ava,i}^{-q} / m_i} \times \frac{V_{dc,L}}{R_L} \tag{51}$$

in case of the charge progress, where

$$m_i = R_{VR0} \frac{E_{BT,i}}{E_{\max}} \tag{52}$$

Additionally, it can be assumed that the load current is caused by the increase load represented by the resistance R_L in the discharge progress or the resistance connected parallel with the current source, which represented for the charge progress. Hence $V_{dc,L}$ in discharge and charge can be rewritten respectively as:

$$V_{dc,L} = V_{dcref} - \Delta V_{dc} \tag{53}$$

$$V_{dc,L} = V_{dcref} + \Delta V_{dc} \tag{54}$$

Therefore, the limitation of the maximum permitted DC voltage deviation can be expressed as

$$\frac{1}{\sum\limits_{i=1}^{n} SOC_{ava,i}^{q} / m_i} \times \frac{V_{dcref} - \Delta V_{dc}}{R_L} \leq \Delta V_{dclower} \tag{55}$$

$$\frac{1}{\sum\limits_{i=1}^{n} SOC_{ava,i}^{-q}/m_i} \times \frac{V_{dcref} + \Delta V_{dc}}{R_L} \leq \Delta V_{dcupper} \tag{56}$$

where $\Delta V_{dclower}$ and $\Delta V_{dcupper}$ are the maximum deviation of the DC voltage in the discharge and charge process respectively, and can be calculated as:

$$\Delta V_{dclower} = V_{dcref} - V_{dcmin} \tag{57}$$

$$\Delta V_{dcupper} = V_{dcmax} - V_{dcref} \tag{58}$$

From Inequality (55) and Inequality (56), it yields:

$$\sum_{i=1}^{n} SOC_{ava,i}^{-q}/m_i \geq \frac{V_{dcref} + \Delta V_{dcupper}}{R_L \Delta V_{dcupper}} \tag{59}$$

$$\sum_{i=1}^{n} SOC_{ava,i}^{q}/m_i \geq \frac{1}{R_L} \times \frac{V_{dcref}}{\Delta V_{dclower}} \tag{60}$$

It is obviously seen that $\sum SOC_{ava,i}^{q}$ is a decreasing function of q, when other parameters are assumed as constant. Thus, inequality (59) and (60) will pose the upper and lower limit for the exponent coefficient. It is understandable because of the functions determining the AVR in charge and discharge. It is seen that when q increases the AVR in discharge will increase, thus it leads to larger DC voltage deviation. In contrast, when q decreases the AVR in the charge will increase, thus also leading to larger DC voltage deviation. This makes two objectives conflicted. Hence, the tradeoff can be made to choose the coefficient q.

(3) On other hand, the lower limit of the exponent coefficient is determined by minimizing the difference of SOCs within the acceptable time duration. Generally, it is assumed that the SOC_i and SOC_k are the highest SOC and lowest SOC among all BESSs respectively. From (4), taking the derivative of SOC_i and SOC_k, it can be derived as.

$$\frac{\partial SOC_\alpha}{\partial t} \times \frac{1}{SOC_{ava,\alpha}^{q}} = \frac{\partial SOC_\beta}{\partial t} \times K \times \frac{1}{SOC_{ava,\beta}^{q}} \tag{61}$$

where K is expressed as:

$$K = \frac{\eta_1 R_{VR0,i}}{\eta_2 R_{VR,k}} \tag{62}$$

It is noted that q is chosen larger than 1 because of improving the SOC-balancing speed. Hence, by solving the differential Equation (61), it yields

$$\left(\frac{SOC_{ava,\alpha}}{SOC_{ava,\beta}}\right)^{1-q} = K + \frac{(SOC_{ava,\alpha}^{1-q} - K \times SOC_{ava,\beta}^{1-q})|_{t=0}}{SOC_{ava,\beta}^{1-q}} \tag{63}$$

It is desired that after the scheduled time duration T, the difference between SOC_i and SOC_k is smaller than ε. In other word, ε is the variable representing the SOC-balancing accuracy. The acceptable SOC-balancing accuracy ε should be obtained within the time duration T. Then, it yields:

$$(SOC_{ava,\alpha}/SOC_{ava,\beta})|_{t=T} \leq 1 + \xi \tag{64}$$

From Equation (64) it can be rewritten as

$$((SOC_i - SOC_{\min}) - (SOC_k - SOC_{\min}))|_{t=T} \leq \varepsilon \tag{65}$$

$$\frac{SOC_{ava,i}}{SOC_{ava,k}}|_{t=T} \leq 1 + \varepsilon \tag{66}$$

It is also noted that

$$(SOC_{ava,\alpha}/SOC_{ava,\beta})|_{t=T} \geq 1 \text{ and } 1 - q < 0 \tag{67}$$

Therefore, from Equation (63) and Inequality (66), it can be drawn that

$$(1 + \xi)^{1-q} \leq K + \frac{(SOC_{ava,\alpha}^{1-q} - K \times SOC_{ava,\beta}^{1-q})|_{t=0}}{SOC_{ava,\beta}^{1-q}|_{t=T}} \tag{68}$$

Consequently, the lower limitation of the *q* can be achieved by solving the constraint (68).

A case study is presented as an instance of determining the limitation range of the exponent coefficient *q*. The parameters of the case study are listed in the Appendix A. It is assumed that SOC_1 and SOC_2 are initially at 0.9 and 0.8. Two *BESSs* supply the load of 600 kW. The desired time to get the equalization of *SOCs* is: *T* = 5000 s with the error of ε = 0.01. As a result, the lower limit of the *q* achieved from solving inequality (68) is 0, while considering the constraint (59) causing by maximum voltage deviation is 1. The upper limit of the *q* considering the constraint (60) is 7, while considering the constraint (49) is 9. Therefore, the proper range of the *q* is $1 \leq q \leq 7$. It should be noted that the BESSs should operate with SOC in the proper range from SOC_{low} to SOC_{high}. Due to the proposed method, the BESSs will automatically avoid to conflicting the technical limit.

5. Small Signal Analysis

In order to study the effects of the adaptive control method on the stability of the system, it is necessary to firstly linearize the nonlinear models such as WECS, BESS including the adaptive droop control before analysis. The small signal model of the DC distribution as is taken on [38]. The state equations of the system in Figure 1 can be properly written in term of the matrix form as in Equation (69) and the output of the system is defined as Equation (70) bellows:

$$\dot{x} = f(x, u, t) \tag{69}$$

$$y = g(x, u, t) \tag{70}$$

It is supposed that the DC grid is operating at a steady-state point where two BESS discharge the load of 400 kW. Linearizing the state equations of the system including the proposed method applied for BESS around the steady-state operating point, the small-signal model of the system can be defined as follows:

$$\dot{\widetilde{x}} = A\widetilde{x} + B\widetilde{u} \tag{71}$$

$$\widetilde{y} = C\widetilde{x} + D\widetilde{u} \tag{72}$$

where $\widetilde{x} = x - x_s$; $\widetilde{u} = u - u_s$ and $\widetilde{y} = y - y_s$ and where the subscript "s" denotes the steady-state values and matrix *A*, *B*, *C* and *D* are defined as:

$A = \frac{\partial f}{\partial x}|_{x_s, u_s}$; $B = \frac{\partial f}{\partial u}|_{x_s, u_s}$; $C = \frac{\partial g}{\partial x}|_{x_s, u_s}$ and $D = \frac{\partial g}{\partial u}|_{x_s, u_s}$. Based on matrix *A*, *B*, *C* and *D*, the eigenvalues of the system can be calculated. The characteristic equation of A is defined as:

$$\det(A - \lambda I) = 0 \tag{73}$$

where *I* is an identity matrix of appropriate dimensions and λ is the system eigenvalues of the matrix A.

In order to observe the influence of the proposed method on the stability, two cases are analyzed, which are shown in Figure 7. Figure 7a shows the dominant eigenvalue locus when the coefficient *q* increased from 1 to 7 as in the proper range found in the previous section. It can be seen that the movement of the most critical pole is toward the right plane. The stable margin of the system is thus

decreased. However, it is noted that this does not cause further oscillations. The impact of different SOCs on the stability is depicted on Figure 7b. It is obviously seen that when the SOCs decrease, the stability margin is also deceased due to the increase of the AVR in the discharge progress.
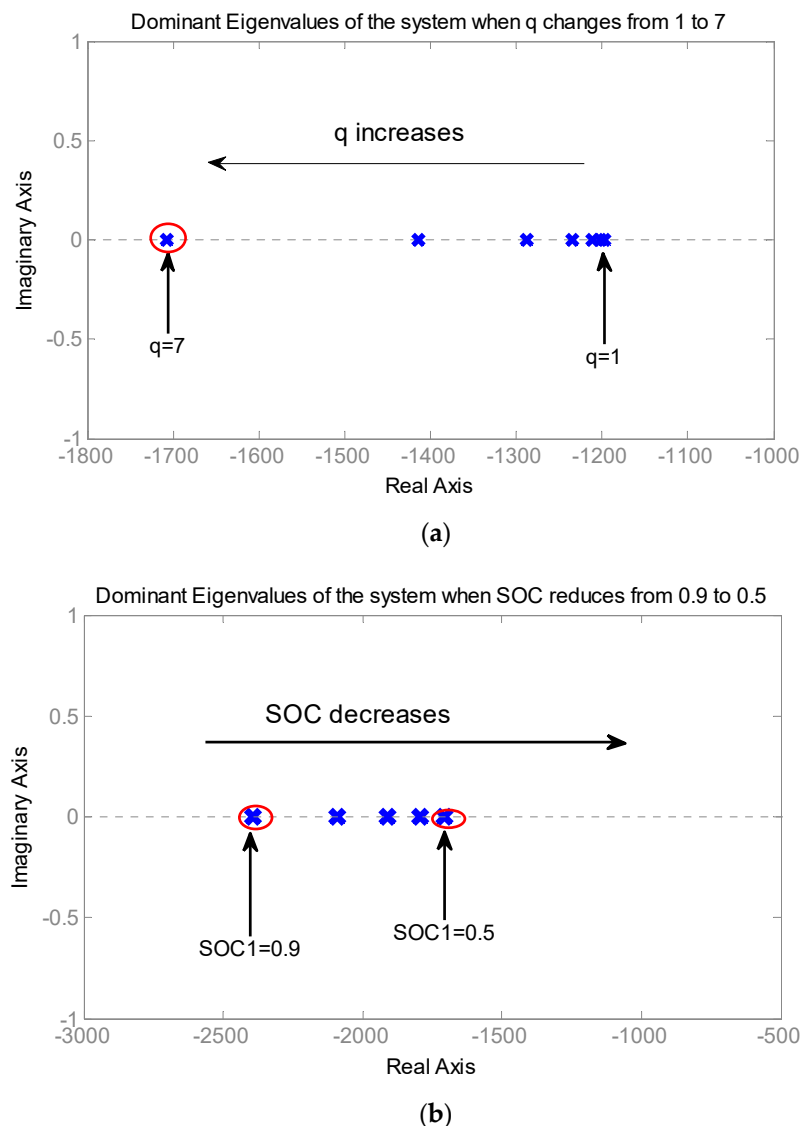

(**a**)

(**b**)

Figure 7. Dominant eigenvalues of the system. (**a**) Root locus with change of *q* and (**b**) root locus with change of SOC.

6. Simulation Results and Discussion

The proposed adaptive droop method was realized by simulation in Matlab and PSCAD [39]. The parameters of the system as in Figure 1 are provided in the Appendix A. The long-term operation of the system is performed in Matlab. The transient responses during contingency were simulated in PSCAD.

For the conventional droop control, the ΔV_{dcmax} of all BESSs were ±10 V. The AC grid converter was activated when the voltage deviation within ±9 V ÷ 19 V. The permitted minimum *SOC* and SOC_{low} in this operation period of all BESSs was 0.2 and 0.5 to get an illustrative example. Other parameters of the system are given in the Appendix A. From case 1 to case 4, only two BESSs were considered. In case 5, three BESSs were considered.

6.1. Performance of the Proposed Control Method in Long-Term Operation

Case 1: Performance of the adaptive control with a different exponent coefficient

The SOCs and output powers of BESSs are shown in Figure 8 with the assumption that two BESSs discharge the load of 400 kW. The real-time SOC_1 and SOC_2 at the starting point were 0.9 and 0.8 respectively. It means that the corresponding available energy levels of $BESS_1$ and $BESS_2$ were 0.7 and 0.6. It is seen that larger q led to shorter time for achieving the SOC-balance, thus faster equalization of the output powers of BESSs.
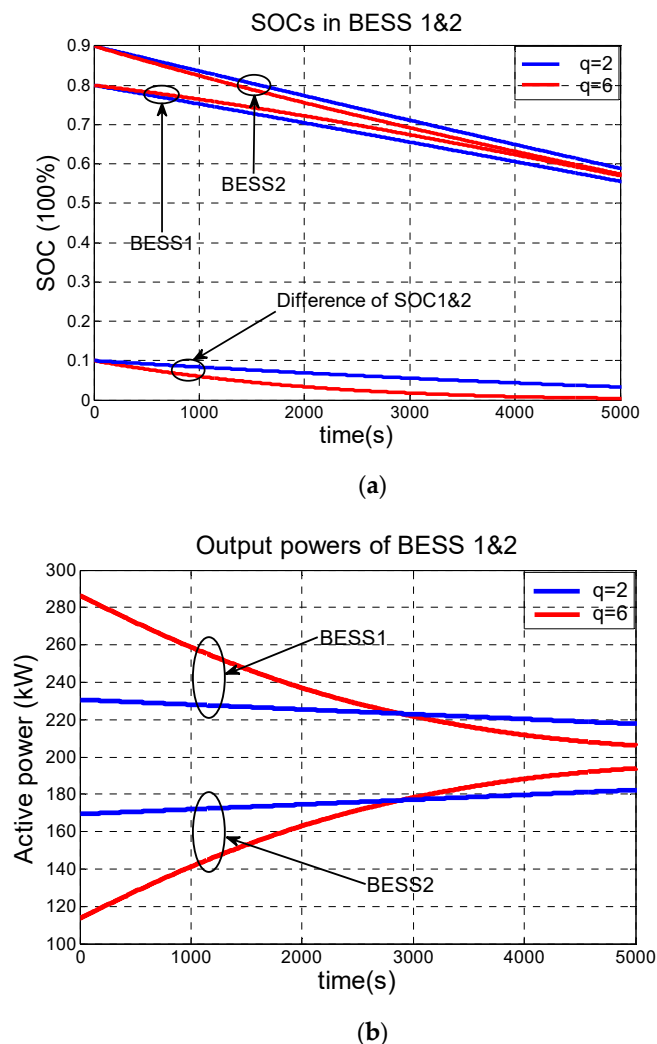
(**a**)

(**b**)

Figure 8. SOC and power sharing waveforms for the adaptive control with different q. (**a**) Waveforms of SOCs and (**b**) waveforms of output powers of BESSs.

Case 2: Performance of the adaptive control with different initial SOCs

In the first test case, the difference between SOC_1 and SOC_2 was 0.1. In order to validate the proposed method with range of difference SOCs, the initial SOC_1 was fixed 0.9 and the initial SOC_2 was changed from 0.8 to 0.4. Difference initial SOCs will lead to different available energy levels of SOCs. As seen in Figure 9, the validation of the adaptive droop control was realized with various available energy levels. It is seen that equalization of SOCs could be achieved with this method. Additionally, the power sharing of BESS 1 and 2 was consistent with the available energy levels in each BESS.
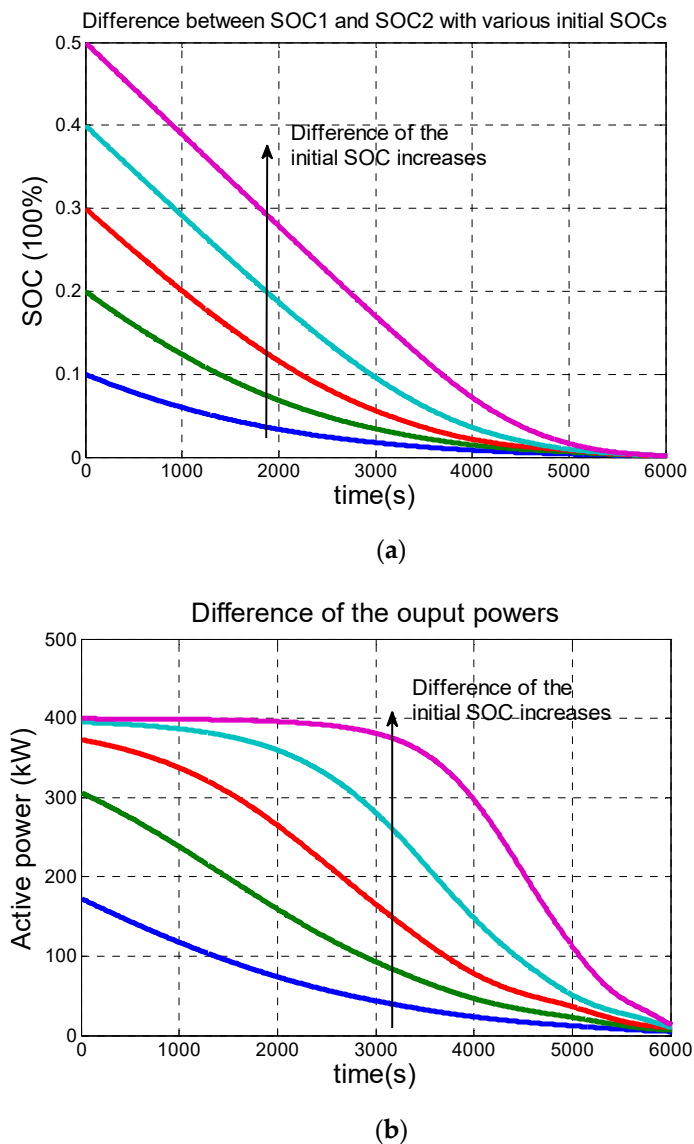
(**a**)

(**b**)

Figure 9. Waveforms of the SOC difference and output power difference with various initial SOCs.
(**a**) Waveforms of the SOC difference and (**b**) output power difference.

Case 3: Validation of the adaptive control with consideration of the estimated errors

It is reported that there is error in the estimation of SOC [33]. Therefore, the method should be tested with consideration of an estimated error of SOC. In Figure 10, the waveforms of SOCs and output powers of BESSs are depicted. It is seen that the proposed method was valid for different errors.
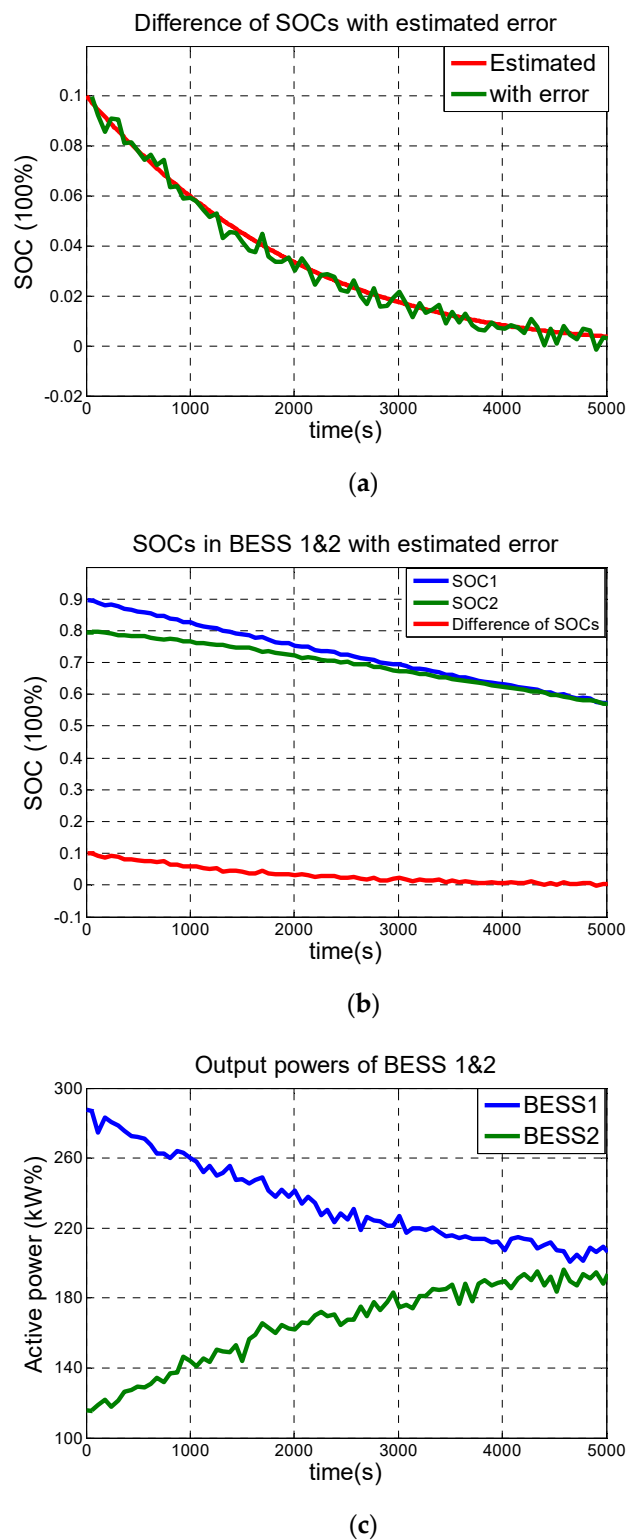
(**a**)

(**b**)

(**c**)

Figure 10. SOC and power sharing waveforms with consideration estimated errors. (**a**) Waveforms of SOC estimated and with errors; (**b**) waveforms of SOCs with errors and (**c**) waveforms of output powers with estimated errors.
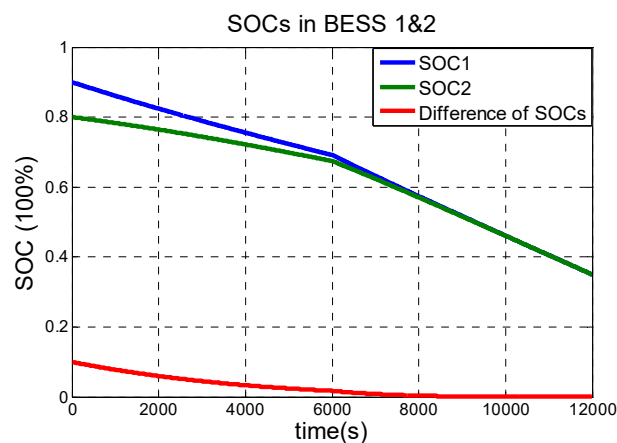
Case 4: Validation of the adaptive control with different loads

Figure 11 shows the power sharing and SOC waveform of BESSs with various loads. It is assumed that the initial load of the system was 200 kW and at the time of 6000 s, the load was increased to

400 kW. At the beginning, the SOC_1 and SOC_2 were 0.9 and 0.8 respectively. The output powers of $BESS_1$ and $BESS_2$ were 111 kW, 89 kW. After the change of load, the output powers of $BESS_1$ and $BESS_2$ were 221.6 kW and 178.4 kW, which it is noted that the power sharing of BESSs was consistent with the analytical derivation (46). The dynamics of the system when changing the load were also investigated in real-time simulation, which will be presented in Section 6.2. It is also noted that the results obtained from this case in the long-term operation would be used for real-time simulation.
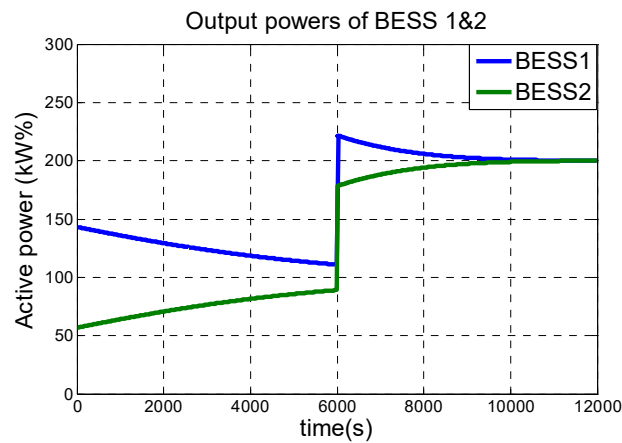
(**a**)

(**b**)

Figure 11. SOC and output power waveforms in case of a change of load at a time of 6000 s. (**a**) Waveforms of SOC and (**b**) waveforms of output powers.

Case 5: Validation of the adaptive control considering disturbance happening suddenly in the grid

It was chosen that the system had three BESSs in order to get an illustrative example for verification of the proposed method. It was assumed that there would be an outage of $BESS_1$ at a time of 2000 s. Figure 12 depicts the waveforms of SOC and power sharing of BESSs. At the time occurring outage, the SOC 1 and 2 and 3 were 0.829, 0.747 and 0.576 and the output powers of BESS 1, 2 and 3 were 190, 143 and 67 kW correspondingly. After the outage of $BESS_1$, the power sharing between $BESS_1$ and $BESS_2$ were 272 kW and 128kW, which were also consistent with the analytical derivation (46). It is also noted that the results obtained from this case in long-term operation would be used for real-time simulation.
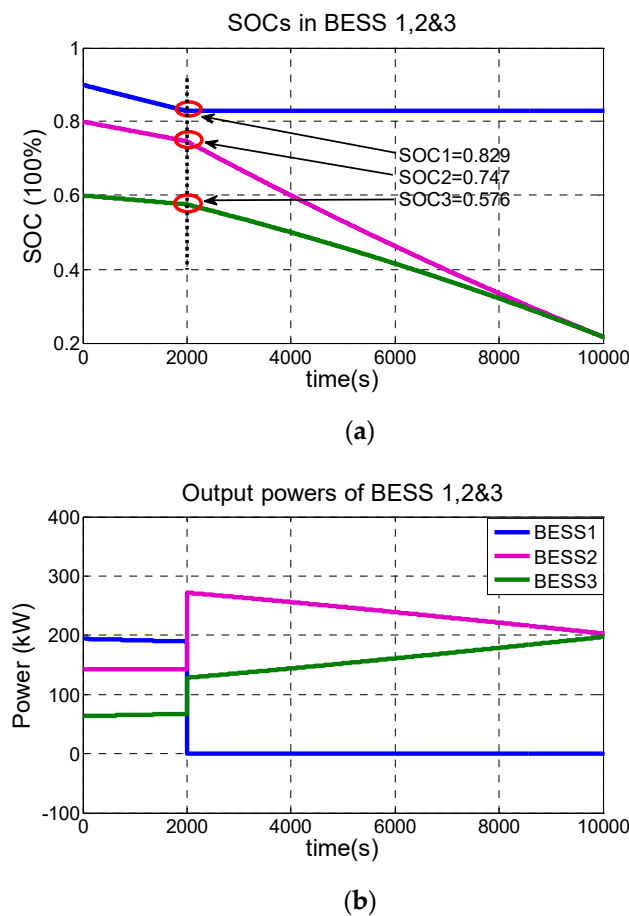
(**a**)

(**b**)

Figure 12. SOC and output waveforms in case of outage of BESS$_1$. (**a**) Waveforms of SOCs and (**b**) waveforms of output powers.

6.2. Validation of the Proposed Control Method on DC Voltage Stabilization during Dynamics

The DC microgrid as shown in Figure 1 was simulated in two representative cases to validate the proposed adaptive control on stabilizing the DC voltages during disturbances for instance a sudden increase of load and an outage of *BESS$_1$*. For the adaptive control, *q* was chosen as 2. The super-capacitor was used to catch fast fluctuations of power by using the cache control as detailed in [34].

Case 1: Change of load from 200 to 400 kW

In order to observe the real-time performance of the presented method, 20 s around the time of 6000 s in case 4 in the long-term operation were run. All parameters were kept the same. The transients of the system are depicted in Figure 13. Before the time of 20 s, with the adaptive droop control, the SOC$_1$ and SOC$_2$ were 0.692 and 0.675, which means the available energy levels of BESS$_1$ and BESS$_2$ were 0.492 and 0.475 respectively, while the output power of BESS$_1$ and BESS$_2$ were 111 kW and 89 kW. These results were also consistent with (46). After the change of load happening, the output powers of BESS 1 and 2 were 221.6 kW and 178.4 kW respectively, which were also consistent with the simulation results in long-term operation and analytical derivations (46). It is drawn that the simulation results in PSCAD were consistent with those in the long-term operation. It can be seen from Figure 13 that the proposed adaptive control provided a slightly better DC voltage profile. The power from PV was kept constant during the 20 s period. The WECS was operated in the MPPT scheme, thus the wind power could be exploited. Due to the supercapacitor, the fast fluctuations could be compensated.
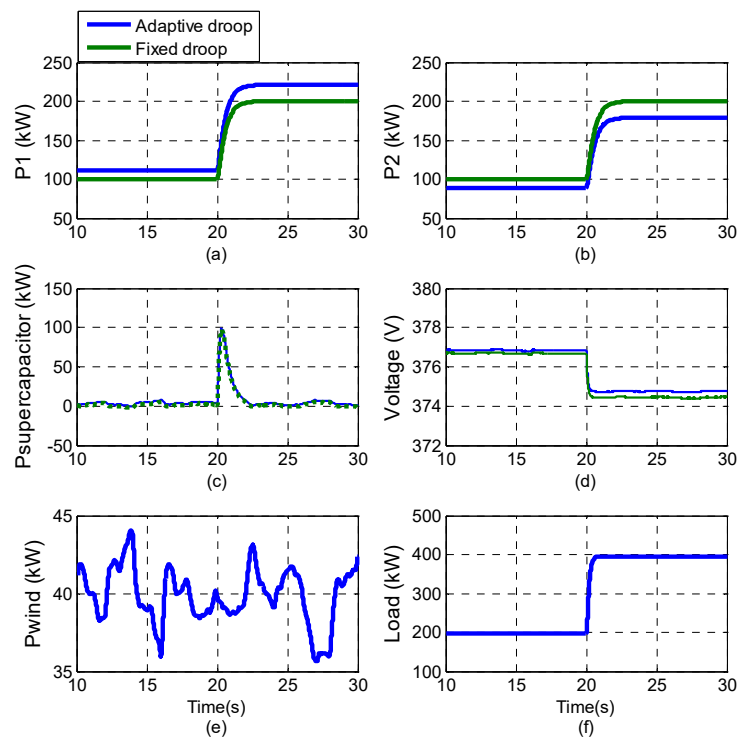
Figure 13. Transients of the system when the load is changed from 200 to 400 kW. (**a**) Output power of BESS$_1$; (**b**) Output power of BESS$_2$; (**c**) Output power of Supercapacitor; (**d**) DC voltage; (**e**) Output power of wind unit and (**f**) Load profile.

Case 2: Outage of BESS$_1$

In this case, the DC system was simulated during 20 s around the time of 2000 s in case 5, in the long-term operation of the previous Section A. Before the outage of BESS$_1$, the SOC$_1$, SOC$_2$ and SOC$_3$ were 0.829, 0.747 and 0.576 respectively and it led to the output powers of BESS1, BESS$_2$ and BESS$_3$ are 190 kW, 143 kW and 67 kW according to the adaptive control. The outage of BESS$_1$ was assumed to be happening at a time of 20 s because it would be the worst case. It is obviously seen in Figure 14 that with the fixed droop control, the output powers of all BESSs were equal. However, it can be seen that with the adaptive droop control, the post-disturbance output powers of BESS$_2$, BESS$_3$ were 272 kW and 128 kW respectively because the power sharing was dependent on the available energy levels of each BESSs, which in this particular case were 0.547 and 0.376 corresponding to BESS$_2$ and BESS$_3$ respectively. It is also seen that the DC voltage profile with the adaptive control was much better than that of the conventional droop control. This is due to large available energy amounts in BESS$_2$ and BESS$_3$. It is noted that in this case, the available energy levels were higher than those in the first case with an increase of load, thus it resulted in the much tighter DC voltage.
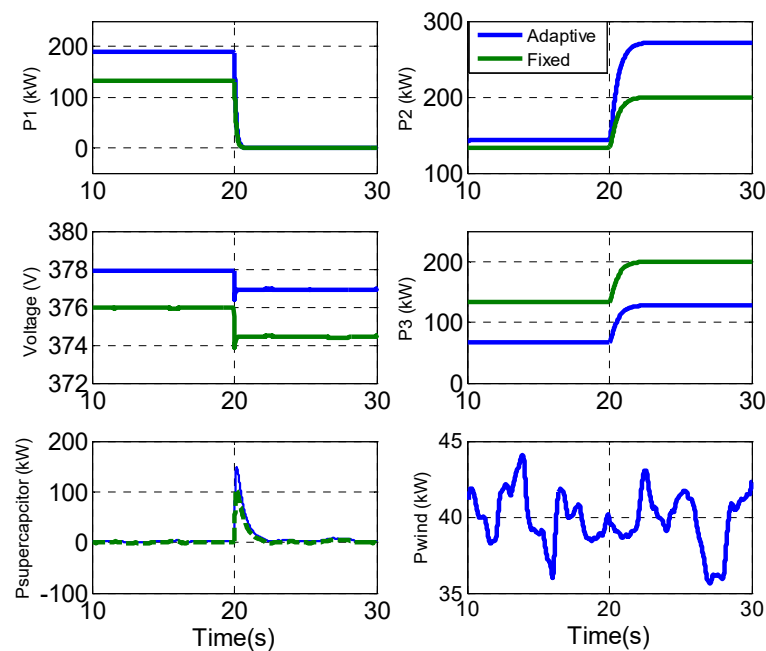
Figure 14. Transients of the system when an outage of BESS$_1$ happens.

7. Conclusions

An available energy level-based adaptive coordinated droop control approach was proposed. This led to the optimal utilization of BESSs for DC grid application. The merit of the adaptive control was established through analytical derivations and validated by simulations for long-term and transient responses. Those simulation results were consistent with those derived analytically. Furthermore, the SOC-balancing speed was also increased due to using the exponent function and automatically adjusted according to the real-time SOC. With this method, the BESS with a higher available energy level will dispatch more power and absorb less power, while the ones with a lower energy level will deliver less power and absorb more power corresponding to the discharge and charge process respectively. The small signal model considering the adaptive coordinated control method was developed to analyze the stability of the system. The proper selection of the exponent coefficients will be analyzed according to the limitations with respect to the maximum permitted current of each converter, the maximum acceptable DC voltage deviation and the small signal analysis. It is shown that there were some conflict criteria for choosing the exponent *q*. It might be that optimization routine should be performed to select the optimal *q*. The proposed droop method is effective due to the dual goals, which are the stabilization of DC voltages especially through disturbance for instance outage of BESS and increase of SOC-balance speed among BESSs, thus optimal utilizing of each BESS. This method can be applied for AC grids with multi-BESSs.

Conflicts of Interest: The author declares no conflict of interest.

Appendix A

Table A1. Parameters of the DC microgrid (as shown in Figure 1).

Notation	Value	Notation	Value	Notation	Value
Parameters of DL block					
R_{12}	0.064 Ω	L_{12}	0.255 mH	C_{12}	10.7 nF
R_{23}	0.064 Ω	L_{23}	0.255 mH	C_{23}	10.7 nF
R_{34}	0.064 Ω	L_{34}	0.255 mH	C_{34}	10.7 nF
R_{41}	0.064 Ω	L_{41}	0.255 mH	C_{42}	10.7 nF
Parameters of PV block					
L_{ddPV}	1mH	C_{dcPV}	5mF	K_{PV}	0.01/V
V_{dcref}	380V				
Parameters of WT block					
R_t	5 m/s	ρ	1.205 kg/m^3	V_{wrated}	12 m/s
K_{popt}	7.87 W/(rad/s)^3	C_{pmax}	0.4412	$P_{genrated}$	36 kW
ω_{rrated}	16.6 rad/s	P	2	H	0.05 s
Ψ_f	90 Wb	L_{md}	0.334 H	L_{mq}	0.217 H
L_{ls}	0.0344 H	R_s	0.08 Ω	K_{p1}	1.01/A
K_{i1}	2.21/A.s	K_{p2a}	5 A/rad	K_{i2a}	150 A/rad.s
K_{p2b}	1.01/A	K_{i2b}	2.21/A.s	K_{p3}	2 deg/rad
K_{i3}	4 deg/rad.s	C_{dcWT}	5mF		
Parameters of BT + SC block					
L_{ddBT}	120 mH	C_{dcBT}	5 mH	R_{1BT}	0.1 Ω
R_{2BT}	0.075 Ω	R_{pBT}	25×10^6 Ω	C_{1BT}	500 F
C_{bBT}	300 (F)	K_{p4aBT}	1 A/V	K_{i4aBT}	5 A/V.s
K_{p4bBT}	0.3/A	K_{i4bBT}	2/A.s	V_{dcref}	380 V
E_{BT}	1000 kWh	P_{rateBT}	400 kW	P_{rateSc}	200 kW

References

1. Natori, K. Overview and perspective of dispersed generation systems. *IEEE J. Trans. Power Energy* **2000**, *120*, 787–790. [CrossRef]
2. Yokoyama, A. Trends and forecasts for novel electric network system. *IEEE Trans. Jpn.* **2005**, *125*, 145–148.
3. Boroyevich, D.; Cvetkovic, I.; Dong, N.; Burgos, R.; Wang, F.; Lee, F. Future electronic power distribution systems a contemplative view. In Proceedings of the 2010 12th International Conference on Optimization of Electrical and Electronic Equipment, Brasov, Romania, 20–22 May 2010; pp. 1369–1380.
4. Chiba, Y.; Marif, Y.; Boukaoud, A.; Meredef, L.; Kaidi, Y. Impact of green buildings on HVAC system located in Algeria. In Proceedings of the 2018 International Conference on Applied Smart Systems (ICASS), Medea, Algeria, 24–25 November 2018; pp. 1–4.
5. Cai, W.; Wu, Z.; Wang, H. Effect of green roof on urban human settlement and indoor environment for green buildings. In Proceedings of the 2011 International Conference on Electric Technology and Civil Engineering (ICETCE), Lushan, China, 22–24 April 2011; pp. 3102–3105.
6. Amran, M.E.; Muhtazaruddin, M.N.; Kamaruddin, S.A.; Muhammad-Sukki, F.; Abu-Bakar, S.H.; Ayub, A.S.; Bani, N.A.; Saudi, A.S.M.; Ardila-Rey, J.A. Renewable energy performance of the green buildings: Key-enabler on useful consumption yield. *IEEE Access* **2020**, *8*, 95747–95767. [CrossRef]
7. Giraud, F.; Salameh, Z. Steady-state performance of a grid-connected rooftop hybrid wind-photovoltaic power system with battery storage. *IEEE Trans. Energy Convers.* **2001**, *16*, 1–7. [CrossRef]
8. Borowy, B.; Salameh, Z. Methodology for optimally sizing the combination of a battery bank and PV array in a wind/PV hybrid system. *IEEE Trans. Energy Convers.* **1996**, *11*, 367–375. [CrossRef]
9. Ito, Y.; Sugita, T.; Yang, Z. DC-bus-connected distribution power system. *PE SOC. Annu. Conf.* **2002**, *1*, 311–612.

10. Daniel, N.; Ambra, S. Efficiency analysis of low-and medium-voltage dc distribution systems. In Proceedings of the IEEE Power Engineering Society General Meeting, Denver, CO, USA, 6–10 June 2004.

11. Brenna, M.; Tironi, E.; Ubezio, G. Proposal of a local DC distribution network with distributed energy resources. In Proceedings of the 2004 11th International Conference on Harmonics and Quality of Power (IEEE Cat. No.04EX951), Lake Placid, NY, USA, 12–15 September 2005; pp. 397–402.

12. Srivastava, A.K.; Bastos, J.L.; Schulz, N.; Ginn, H.L. AC/DC power system modeling and analysis for shipboard applications. In Proceedings of the 2007 IEEE Power Engineering Society General Meeting, Tampa, FL, USA, 23 July 2007; pp. 1–5.

13. El-Samahy, I.; El-Saadany, E. The effect of DG on power quality in a deregulated environment. *IEEE Power Eng. SOC. Gen. Meet.* **2005**, *3*, 714–721. [CrossRef]

14. Khatri, P.R.; Jape, V.S.; Lokhande, N.M.; Motling, B.S. Improving power quality by distributed generation. In Proceedings of the Power Engineering Conference, IPEC'05, Singapore, 29 November–2 December 2005; pp. 675–678.

15. Guerrero, J.M.; Vasquez, J.C.; Matas, J.; de Vicuña, G.G.; Castilla, M. Hierarchical control of droop-controlled AC and DC microgrids—A general approach toward standardization. *IEEE Trans. Ind. Electron.* **2011**, *58*, 158–172. [CrossRef]

16. Lu, X.; Guerrero, J.M.; Sun, K.; Vasquez, J.C.; Teodorescu, R.; Huang, L. Hierarchical control of parallel AC-DC converter interfaces for hybrid microgrids. *IEEE Trans. Smart Grid* **2013**, *5*, 683–692. [CrossRef]

17. Dong, D.; Cvetkovic, I.; Boroyevich, D.; Zhang, W.; Wang, R.; Mattavelli, P. Grid-interface bi-directional converter for residential DC distribution systems—Part one: High-density two-stage topology. *IEEE Trans. Power Electron.* **2013**, *28*, 1655–1666. [CrossRef]

18. Kakigano, H.; Miura, Y.; Ise, T. Distribution voltage control for DC microgrids using fuzzy control and gain-scheduling technique. *IEEE Trans. Power Electron.* **2012**, *28*, 2246–2258. [CrossRef]

19. Guerrero, J.M.; Loh, P.C.; Lee, T.-L.; Chandorkar, M. Advanced control architectures for intelligent microgrids—Part II: Power quality, energy storage, and AC/DC microgrids. *IEEE Trans. Ind. Electron.* **2013**, *60*, 1263–1270. [CrossRef]

20. Kim, J.W.; Choi, H.S.; Cho, B.H. A novel droop method for the converter parallel operation. In Proceedings of the 16th Annual IEEE Applied Power Electronics Conference and Exposition, Anaheim, CA, USA, 4–8 March 2001.

21. Lu, X.; Sun, K.; Guerrero, J.M.; Huang, L. SOC-based dynamic power sharing method with AC-bus voltage restoration for microgrid applications. In Proceedings of the IECON 2012—38th Annual Conference on IEEE Industrial Electronics Society, Montreal, QC, Canada, 25–28 October 2012; pp. 5677–5682.

22. Gkavanoudis, S.I.; Oureilidis, K.; Demoulias, C.S. An adaptive droop control method for balancing the SOC of distributed batteries in AC microgrids. In Proceedings of the 2016 IEEE 17th Workshop on Control and Modeling for Power Electronics (COMPEL), Trondheim, Norway, 27–30 June 2016; pp. 1–6.

23. Urtasun, A.; Sanchis, P.; Marroyo, L. Stand-alone AC supply systems with distributed energy storage. *Energy Convers. Manag.* **2015**, *106*, 709–720. [CrossRef]

24. Kakigano, H.; Nishino, A.; Ise, T. Distribution voltage control for DC microgrid with fuzzy control and gain-scheduling control. In Proceedings of the 8th International Conference on Power Electronics-ECCE Asia, Jeju, Korea, 29 May–2 June 2011; pp. 256–263.

25. Ye, Z.; Boroyevich, D.; Xing, K.; Lee, F.C. Design of parallel sources in DC distributed power systems by using gain-scheduling technique. In Proceedings of the 30th Annual IEEE Power Electronics Specialists Conference. Record. (Cat. No.99CH36321), Charleston, SC, USA, 1 July 1999; Volume 1, pp. 161–165.

26. Tsikalakis, A.G.; Hatziargyriou, N.D. Centralized control for optimizing microgrids operation. *IEEE Trans. Energy Convers.* **2008**, *23*, 241–248. [CrossRef]

27. Chaudhuri, N.R.; Chaudhuri, B. Adaptive droop control for effective power sharing in multi-terminal DC (MTDC) grids. *IEEE Trans. Power Syst.* **2013**, *28*, 21–29. [CrossRef]

28. Karlsson, P.; Svensson, J. DC bus voltage control for a distributed power system. *IEEE Trans. Power Electron.* **2003**, *18*, 1405–1412. [CrossRef]

29. Kurohane, K.; Senjyu, T.; Yona, A.; Urasaki, N.; Muhando, B.E.; Funabashi, T. A high quality power supply system with DC smart grid. In Proceedings of the 2010 IEEE PES Transmission and Distribution Conference and Exposition: Smart Solutions for a Changing World, New Orleans, LA, USA, 19–22 April 2010; pp. 1–6.

30. Louie, H.; Strunz, K. Superconducting magnetic energy storage (SMES) for energy cache control in modular distributed hydrogen-electric energy systems. *IEEE Trans. Appl. Supercond.* **2007**, *17*, 2361–2364. [CrossRef]

31. Salameh, Z.M.; Casacca, M.A.; Lynch, A. A mathematical model for lead-acid batteries. *IEEE Trans. Energy Convers.* **1992**, *7*, 93–98. [CrossRef]

32. Strunz, K.; Abbasi, E.; Huu, D.N. DC microgrid for wind and solar power integration. *IEEE J. Emerg. Sel. Top. Power Electron.* **2014**, *2*, 115–126. [CrossRef]

33. He, H.; Xiong, R.; Zhang, X.; Sun, F.; Fan, J. State-of-charge estimation of the lithium-ion battery using an adaptive extended kalman filter based on an improved thevenin model. *IEEE Trans. Veh. Technol.* **2011**, *60*, 1461–1469. [CrossRef]

34. Strunz, K.; Louie, H. Cache energy control for storage: Power system integration and education based on analogies derived from computer engineering. *IEEE Trans. Power Syst.* **2008**, *24*, 12–19. [CrossRef]

35. Duc, N.H. An adaptive control of hybrid battery-supercapacitor storage for integration of wind and solar. In Proceedings of the 2016 IEEE International Conference on Sustainable Energy Technologies (ICSET), Hanoi, Vietnam, 14–16 November 2016.

36. Duc, N.H.; Hung, T.N. Adaptive coordinated droop control for multi-battery storage. In Proceedings of the IEEE Eurocon 2015—International Conference on Computer as a Tool (EUROCON), Salamanca, Spain, 8–11 September 2015.

37. Duc, N.H.; Hung, T.N. DC microgrid for buildings integrated renewable energy sources. *Int. J. Emerg. Res. Manag. Technol.* **2016**, *5*, 12.

38. Duc, N.H. State-Space Modelling and Voltage Control of AC-DC Networks. Ph.D. Thesis, Technical University of Berlin, Berlin, Germany, 2014.

39. *EMTDC Transient Analysis for PSCAD Power System Simulation Version 4.2.0*; Manitoba HVDC Research Centre: Winnipeg, MB, Canada, 2005.